NASA TM X-388

NASA TM X-388

TECHNICAL MEMORANDUM

X-388

DESIGN AND EXPERIMENTAL PERFORMANCE OF A SMALL CENTRIFUGAL PUMP FOR LIQUID HYDROGEN

By George W. Lewis, Edward R. Tysl, and Melvin J. Hartmann

Lewis Research Center
Cleveland, Ohio

NATIONAL AERONAUTICS AND SPACE ADMINISTRATION
WASHINGTON

September 1960

NATIONAL AERONAUTICS AND SPACE ADMINISTRATION

TECHNICAL MEMORANDUM X-388

DESIGN AND EXPERIMENTAL PERFORMANCE OF A SMALL CENTRIFUGAL PUMP FOR LIQUID HYDROGEN*

By George W. Lewis, Edward R. Tysl, and Melvin J. Hartmann

SUMMARY

Radial-bladed centrifugal pumps for liquid hydrogen may be expected to utilize relatively large outlet- to inlet-diameter ratios and large numbers of splitter blades in order to avoid flow reversals along the blade surfaces. A 4-inch-diameter hydrogen pump was designed and experimentally investigated. The design utilized a stream-filament solution adapted from a centrifugal-compressor design which, through an iterative procedure, resulted in passage and blade shapes, number and position of blades, and calculated velocities throughout the pump rotor passage. A 4-inch-diameter shrouded pump rotor was operated at a flow coefficient of 0.2, a pressure coefficient of 0.585, and an indicated hydraulic efficiency of about 0.65. This is a relatively good performance for a small low-specific-speed pump rotor and is taken as an indication that the arbitrary area allowance made for desired velocity distributions is of the right order of magnitude and that reasonably good internal flow conditions were established. An unshrouded model of this pump rotor was also investigated. However, as might be expected when minimum allowable clearance is large compared to the height of the flow passage, a large reduction in performance was experienced compared with the shrouded-pump performance.

INTRODUCTION

Considerable efforts are being exerted to utilize liquid hydrogen as a rocket propellant both in the high-energy chemical system and in the nuclear system. In these applications a pump is necessary to move the liquid hydrogen from the low-pressure tank to the high-pressure thrust chamber or reactor. The fluid properties of liquid hydrogen result in problems in designing pumps with these relatively large pressure rises.

The pressure produced by a pump rotor is proportional to the product of three terms: the fluid density, the pump rotor tip speed, and the

*Title, Unclassified.

tangential velocity (assuming zero inlet tangential velocity). The first term of this product (the fluid density) is very low for liquid hydrogen, being approximately one-fourteenth that of water. Thus, to produce a large pressure rise, a hydrogen-pump rotor must utilize high rotational speeds and/or large changes in fluid tangential velocities. Rotational speed is limited by stress and mechanical problems involving bearings and seals. The change in fluid tangential velocity is limited to prevent fluid losses from becoming prohibitive.

The effect of large changes in fluid tangential velocity merits some further discussion. Fluid losses result from large velocity gradients in the pump rotor passage due to the relative turning of the fluid necessary to obtain large changes in tangential velocity. Large changes in tangential velocity also result in high velocities in the pump volute and must be expected to increase the diffusion losses in this region. Turning the fluid beyond the radial direction results in changes in the slope of the head-flow characteristics, making it difficult to match the pump and the flow systems. Radial outlet pumps with radial blades minimize blade bending stresses due to centrifugal forces and make possible high rotational speeds to obtain the high pump pressure rise required. Thus, a centrifugal pump rotor turning the fluid to the radial direction seems to result in a reasonable design to meet the high head requirements of liquid-hydrogen pumps.

The problems associated with the design and the performance characteristics of a radial outlet pump rotor with radial blades have been investigated at the NASA Lewis Research Center. A pump rotor of 4-inch diameter was designed utilizing centrifugal-compressor design methods to approximate the fluid velocity gradients. Experimental performance characteristics of this pump rotor were determined using liquid hydrogen as the test fluid. The design and performance characteristics are presented in this report.

PUMP ROTOR DESIGN CONSIDERATIONS

In the design of a pump rotor, it is first necessary to establish the pump rotor inlet and exit vector diagrams. Generally, the cavitation requirements set the inlet tip vector diagrams. At the rotor inlet the pressure above the fluid vapor pressure is available for conversion to velocity without cavitation. The inlet flow angle can be optimized to give the highest suction specific speed S, as indicated in reference 1 (all symbols defined in appendix A). However, since in this investigation sufficient pressure will be supplied at the pump inlet to avoid cavitation, no particular cavitation problems are considered. The inlet tip vector diagram (fig. 1(a)) for this design was arbitrarily assigned an angle of $76\frac{1}{2}^{\circ}$, which corresponds to the optimum relative flow angle

necessary to obtain a suction specific speed of about 10,000. Assignment of either tip speed or axial velocity will be sufficient to complete the inlet tip vector diagram.

The tip discharge vector diagram is formed by the relative outlet flow velocity and the design outlet tip speed. Since in this design the relative fluid flow at the rotor discharge is radial, the head developed is determined by the rotor outlet tip speed. The discharge vector diagram for this type of design is illustrated in figure 1(b), in which the average through-flow fluid velocity level has not been established. The effect of the average through-flow velocity on blade-to-blade velocity gradients will be considered later.

General considerations indicate that centrifugal pumps for liquid hydrogen would require radial outlet blades. Because of these radial outlet blades, the pump may require a large change in diameter from inlet to outlet in order to obtain sufficient blade length to maintain flow without excessive velocity gradients. The use of large outlet- to inlet-diameter ratios results in low inlet relative velocities, thus reducing the inlet cavitation problem. Mechanical problems, such as bearing DN numbers and seal surface speeds, are also reduced when large diameter ratios are used. An outlet- to inlet-diameter ratio of 3.5 was set for this pump design (fig. 1(c)).

Several problems arise concerning the fluid velocities in the pump rotor passage. To illustrate these problems, flow in a radial-bladed rotor is shown in figure 2. The driving blade surface develops a pressure higher than the trailing blade surface. The pressures are indicated as + and - regions in figure 2(a) and are the normal pressure distributions required for the rotor to exert a torque on the fluid. An "eddy" condition occurs when the velocity in the high (+) pressure region drops to zero and reverses. This is illustrated by streamlines in one of the passages of figure 2(b) and is discussed in reference 2. This flow reversal would be accompanied by increased losses and unstable conditions. A method of avoiding flow reversals would be the addition of more blade surfaces, as shown in figure 2(c). The addition of splitter blades has the advantage of not increasing the trailing-surface velocities to extreme values; however, the additional surface area does increase friction losses. In the pump rotor designed for this investigation, it was found necessary to utilize a large number of splitter blades and increase the relative flow velocity along the hub of the rotor. The following discussion will outline the assumptions and methods used in the design of the passages for this pump rotor.

The passage design method (refs. 3 and 4) used in this study was developed and used in the design of centrifugal-compressor rotors. This method, using stream-filament technique, gives a knowledge of velocities, pressures, and streamlines in the axial-radial plane and approximate

velocities and pressures on the blade surfaces. Since references 3 and 4 discuss the method in detail, only the major points, iterations, and assumptions for the design are given herein:

(1) A desirable hub shape was chosen as shown in figure 3(a). The inlet hub-to-tip diameter ratio was set at 0.55. This, with the flow coefficient φ and d_o/d_i that were established in the preceding discussion, and assumed values of hydraulic efficiency and slip factor, are sufficient to determine the familiar pump parameter specific speed

$$\left\{ N_S = N \frac{\sqrt{Q}}{(\Delta H)^{3/4}} = \frac{C \sqrt{\left[1 - \left(\frac{r_h}{r_s}\right)_i^2\right] \varphi_1}}{(\eta f_s)^{3/4} \left(\frac{d_o}{d_i}\right)_s^{3/2}} \right\}.$$

(2) A blade mean camber line was described as a parabola plus a straight line when projected on a cylinder; the transition from a parabolic shape to a straight line is located at point A as shown in figure 3(a). Since all blades were radial from point A, the complete blade surface was thus defined. Three blades were used at the inlet. Blade thickness was 5 percent of the inlet passage width and was maintained constant throughout the blade length.

(3) The midpassage relative-velocity distribution shown in figure 3(b) was chosen to exist along the hub.

(4) Using a linear distribution of static pressure from blade to blade, the blade surface velocities along the hub were calculated at various distances through the impeller using the method described in reference 4.

(5) Splitter blades (thickness equal to main blades) were added where the blade pressure-surface velocity became zero. Subsequent computations assumed that the splitter blades and main blades obtain the same pressure distributions.

(6) This computation was repeated at eight equal mass streamlines above the hub section using the results of the previous streamline. The profile of the eighth mass streamline is shown in figure 4. The required position at which splitter blades were started is also indicated on this figure.

The hub and calculated shroud fluid velocities are shown in figure 5. In this figure all velocities have been divided by the fluid relative velocity at the inlet rotor tip $V'_{s,i}$. This velocity ratio has been plotted against the percent of flow path. The velocity distribution

along the rotor hub is shown as dashed curves, whereas the velocity distribution along the rotor shroud is shown as solid lines. The hub midpassage velocity, which was varied until suitable design conditions were established, shows a decrease from 0.58 to 0.43 over the first 20 percent of the passage length and then increases to become coincidental with the shroud mean velocity. The blade surface velocities have been faired, especially in the regions where splitter blades were added, since the solution does not account for flow adjustment upstream and near the leading edge of the added blades. On both the trailing and driving surfaces, decreasing velocities occur, followed by an increasing velocity, with the calculated relative velocity on the blade driving surface finally falling off to zero. In the latter portion of the passage the calculations indicate large differences in velocity from the driving to the trailing surfaces. In the real case, however, as the fluid leaves the rotor it must adjust to a uniform flow some distance downstream. This adjustment is felt in the latter portion of the pump rotor passage; thus, there will be a reduction in this large cross-channel velocity difference. This adjustment is not indicated by the design method used for this pump rotor.

The midpassage relative fluid velocity at the shroud decreases from 1.0 to 0.88 at about 30-percent flow-path length, after which this velocity increases to about 0.91 at 40 percent of flow-path length and gradually drops off to 0.725 at the exit. Thus, along the shroud the fluid has encountered an overall decrease in midpassage velocity from 1.0 to 0.725, whereas the hub velocity has experienced an overall acceleration from 0.58 to 0.725. The midpassage relative velocities become coincidental in the latter part of the passage as the effect of the axial-radial streamline curvature is no longer felt. The blade driving-surface velocities indicate that along the shroud the velocity ratio decreased continuously from 1.0 to 0.0 through the machine. The hub driving-face velocity decreases rapidly at first, then increases and approaches the shroud driving-surface velocity contour at about 0.6 passage length. The blade trailing-surface velocities, both hub and shroud, decrease over the first portion of the passage and then increase, becoming coincidental near the blade discharge. All surfaces in the impeller experienced flow deceleration over a portion of the flow path, which contributes to flow losses. The velocity distributions shown in figure 5 were considered acceptable for the rotor used in this investigation. It should be pointed out that several variations of hub shape and hub relative-mean-velocity distributions were investigated before this compromise among velocities, blade numbers, and shroud shape was accepted.

The calculated shroud contour with the location and number of blades for the pump design is shown in figure 6. This passage was calculated on the basis of ideal flow. To obtain the design velocity distributions at the design flow rate, it is necessary to allow some excess

flow area because of ineffective flow regions such as boundary layer that develop within the pump rotor. The magnitude of ineffective flow area is dependent on the ratio of surface area to flow area and the extent of the flow decelerations that are experienced on these surfaces. Thus, for centrifugal pump rotors designed with the general concepts utilized in this investigation, the excess flow area required at the rotor discharge may be dependent mainly on the ratio of surface area to flow area. In NACA centrifugal-compressor research (ref. 5), optimum performance was obtained at excess flow areas 0.4 to 0.7. These compressors had a diameter ratio of about 2. The ratio of surface area to flow area varies roughly as the outlet- to inlet-diameter ratio squared. Extrapolation of the reference data to the diameter ratio of 3.5 used in this investigation indicates that an excess area of about 1.3 should be utilized. This more or less arbitrary excess-area allowance was applied linearly along the meridional length from 0 at the inlet to 1.3 at the exit by increasing the hub-to-shroud distance. The resulting shroud is shown in figure 6.

The examination of the design requirements of a radial-bladed pump rotor has indicated several factors. Besides the requirement of flow-passage length, several mechanical factors indicate that fairly large changes between inlet and outlet diameters are desirable. Large numbers of partial blades or splitters are required to hold the blade surface velocities within reasonable limits. The passage design method seems to result in reasonable definition of fluid velocities throughout the pump rotor. Freedom to vary the hub curvature and hub mean-relative-velocity distribution a small amount seems to have resulted in suitable distributions of splitter blades and velocity gradients throughout the rotor passage.

APPARATUS AND METHODS

Pump Rotor

A 4-inch-diameter pump rotor was built utilizing the design information described in the preceding section. The pertinent dimensions of this impeller are shown in the sketch of figure 7. For this size pump rotor, the blade height at discharge is 0.048 inch, and the blade thickness is 0.061 inch. Hub and shroud coordinates are tabulated in figure 7. Since all blade elements are radial, the blade mean line can be given as indicated by z-θ coordinates on the sketch and table of figure 7.

A photograph of the pump rotors with and without the attached rotating shroud is shown in figure 8. The unshrouded rotor indicates the three full blades from inlet to outlet and the addition of splitter blades until a total of 36 blades exist over the outer portion of the rotor. The shrouded rotor was machined from stainless steel with a

stainless-steel shroud furnace-brazed to the blade tips. The unshrouded rotor was machined from aluminum. This pump was operated with about 0.006-inch axial clearance at the rotor exit between the blade and the Teflon stationary shroud.

Test Facility

A schematic diagram of the test loop used in this investigation is shown in figure 9. A 1000-gallon vacuum-jacketed transportable Dewar was used as a liquid-hydrogen tank. The flow path of hydrogen was from the Dewar to the test pump, through a Venturi mounted in the piping, a throttle valve, and back into the Dewar. Shutoff valves were placed in the pump inlet and discharge piping. Piping in the test loop was vacuum-jacketed with an inside diameter of 1.5 inches with suitable flexible sections. All valves in the test loop were vacuum-jacketed and remote-controlled. Connections to a hydrogen-gas vent system were made through remote-control valves to the Dewar, pump assembly, and between adjacent valves in the test loop.

For safety reasons, an overriding adjustable pressure switch operated these vent valves, and a burst disk was installed around each valve. The vent lines were connected to a 6-inch-diameter vent manifold that extended 300 feet from all equipment to a gas burner. The burner was provided with an automatic pilot flame, and for further safety a small nitrogen-gas flow was maintained through the vent manifold. Other auxiliary systems include a helium-gas supply and vacuum connection for purging the test loop, and a hydrogen-gas supply system for pressurizing the Dewar. Operational and mechanical experiences obtained in this investigation are presented in appendix B.

The pump assembly is shown in the detailed sketch of figure 10. It consists of a cantilevered vertical pump arrangement having two ball bearings and three carbon face seals. The pump rotor utilizes a carbon face seal on the front face of the rotor to prevent backflow between the pump outer shroud and stationary housing. In order to minimize heat transfer to the working fluid, the pump package was immersed in a tank of liquid hydrogen kept at a constant level and atmospheric pressure. The tank of liquid hydrogen and the pump bearing housing were vacuum-jacketed as shown in figure 10.

A commercial air turbine was used to drive the pump. The turbine was powered by the service air system and exhausted to the atmosphere.

Instrumentation

All pressure measurements were taken by pressure transducers. In order to assure that no liquid hydrogen reached the pressure transducer, a length of tubing was used to connect each transducer to the rig. Carbon resistors, approximately 0.07 inch in diameter and 0.15 inch long, were used to measure temperatures because their resistance increases exponentially as temperature decreases in this temperature range. These carbon resistors were stabilized by special processing and cycling between normal and low temperature. The resistors were checked and calibrated periodically.

Pump inlet instrumentation consisted of three shielded carbon resistor probes (fig. 11(a)) and wall static-pressure taps. Pump discharge pressure was obtained by a static wall tap in the torus. A temperature probe located about 2 feet from the torus collector in the jacketed piping measured the temperature of the liquid entering the Venturi flowmeter. Total pressure ahead of the Venturi throat was also obtained in order to compute flow rate. Pump speed was measured by a magnetic-type speed pickup and electronic counter.

Liquid level in the vent lines was indicated by carbon resistor probes (fig. 11(b)). Two level probes (spaced 1 in. apart) were set to control automatically the level of liquid hydrogen in the pump cold bath.

DISCUSSION OF PUMP ROTOR PERFORMANCE

Both the shrouded and unshrouded pump rotors were operated in liquid hydrogen. The experimental results are presented in this section.

The performance of the 4-inch radial-bladed shrouded pump rotor in liquid hydrogen is shown in figure 12. The pressure rise developed for constant rotational tip speeds of 196, 274, 353, and 392 feet per second is shown over the range of flows obtained in this investigation. The curve for the data point obtained at a tip speed of 392 feet per second is the corrected average data obtained at the lower speeds. In general, for a given speed the pressure rise is constant over a range of flow rates and falls off at the low end of the flow range. This decrease in pressure rise is due to a reduction in tangential velocity imparted to the fluid (an increase in slip factor f_s) and/or an increase in fluid losses in passing through the rotor. In this case, probably both factors combine to result in the reduced pressure rise in the low-flow region. At a tip speed of 392 feet per second a pressure rise of about 82 pounds per square inch was obtained at a flow of 56 gallons per minute. This corresponds to a head rise of about 2690 feet of hydrogen.

Head coefficient ψ is plotted against flow coefficient φ in figure 13. Above a flow coefficient of 0.2 the head coefficient is 0.585. Below a flow coefficient of 0.2 the head coefficient falls off rapidly. The head coefficient for a radial outlet pump is equal to the product of slip factor and pump efficiency. If a slip factor of 0.9 is assumed (ref. 6) for values of flow coefficients above 0.2, the hydraulic efficiency of this pump would be in the order of 0.65. Since the specific speed N_S of this pump at the design flow coefficient of 0.24 is only about 420, this is thought to be a reasonably good hydraulic efficiency.

Because the experimental performance is relatively good, it can be presumed that the relative velocity gradients obtained in this pump rotor approached design values. Since no data were obtained to determine the velocity gradients that exist in this rotor, the design velocity gradients cannot be checked, and the assumption of an excess area of 1.3 at the rotor discharge cannot be evaluated. It should be pointed out that the excess-area allowance was made large because of the very large ratio of friction surface area to flow area of this pump rotor. This value may not be typical for pumps having higher specific speeds.

The unshrouded rotor was also experimentally investigated in liquid hydrogen. The head and flow coefficients obtained with the unshrouded rotor are shown in figure 14. The head coefficients generally decrease with increasing flow coefficient. Thus, the shape of head characteristic curve is changed as well as being somewhat lower than that of the shrouded rotor (dashed curve in fig. 14). Thus, the flow out of the unshrouded rotor and the losses experienced by this rotor must be sizably different from those for the shrouded rotor. The running clearance between the blade tips and the stationary shroud was set at 0.012 inch at the rotor inlet and 0.006 inch at the pump discharge. Since at the rotor discharge the blade height was only 0.048 inch, the clearance is about 12 percent of the blade height. Leakage through the clearance space should be expected to have a sizable effect on the resulting flow pattern.

SUMMARY REMARKS

Centrifugal pumps for liquid hydrogen are characterized by radial blading and high rotor tip speed. These factors make liquid-hydrogen pumps somewhat different from pumps for normal high-density liquids. The following remarks can be made concerning this design study and experimental investigation:

1. Since hydrogen pumps require a relatively high head rise, critical velocity gradients are encountered in the rotor passages. In this investigation a stream-filament method was utilized to indicate blade surface

velocities throughout the rotor. A 4-inch-diameter pump rotor required three blades at the pump inlet; and, to avoid zero velocity or flow reversal, successive groups of splitters were added until 36 blades were required in the latter portion of the pump rotor. Even with 36 blades, driving-blade-surface velocities of zero are indicated at the discharge.

2. The design calculations do not define the effect of fluid losses on velocity gradients or the adjustment of the flow to uniform flow conditions near the impeller discharge.

3. The 4-inch-diameter shrouded pump rotor obtained a pressure rise of about 82 pounds per square inch in the flow range from 55 to 70 gallons per minute at a rotor tip speed of 392 feet per second. This is comparable to a pressure coefficient of 0.585 at flow coefficients above 0.2. If this pump rotor were operated at tip speeds approaching stress limits, in the order of a 1200-foot-per-second tip speed, a pressure rise of about 770 pounds per square inch could be expected.

4. One of the major areas of uncertainty was the amount of excess-area allowance to establish the desired velocity distribution. In this 4-inch-diameter rotor with a diameter ratio of 3.5, an excess area of 1.3 times the design flow area was used at the rotor discharge. Since the rotor performance was relatively good, the excess area is probably of the right order of magnitude for this type of rotor. However, it was not possible experimentally to determine the velocity distributions.

5. An unshrouded version of this pump rotor was also operated in liquid hydrogen. A large decrease from performance of the shrouded rotor was obtained. This might have been expected from the fact that the minimum allowable blade tip clearance was large compared with the passage height.

Lewis Research Center
National Aeronautics and Space Administration
Cleveland, Ohio, May 13, 1960

APPENDIX A

SYMBOLS

C	constant
d	diameter, ft
f_s	slip factor, or $\frac{\text{actual tangential velocity}}{\text{ideal tangential velocity}}$
g	acceleration due to gravity, ft/sec^2
H	total pressure head, ft
ΔH	pump head rise, ft
H_{sv}	net positive suction head, $H_i - h_v$
h_v	vapor pressure, ft
N	pump speed, rpm
N_S	specific speed, $N\sqrt{Q}/\Delta H^{3/4}$
ΔP	pump pressure rise, lb/sq in.
Q	flow rate, gpm
r	radius measured from axis of rotation, ft
S	suction specific speed, $N\sqrt{Q}/H_{sv}^{3/4}$
U	pump tip speed, ft/sec
V	velocity, ft/sec
z	axial length, ft
η	efficiency
θ	circumferential angle, deg
φ	flow coefficient, $\left\lvert\frac{V_z}{U}\right\rvert_i$
Ψ	head coefficient, $g\Delta H/U_o^2$

[redacted]

Subscripts:

h	pump rotor hub
i	pump rotor inlet
o	pump rotor outlet
s	shroud
z	axial direction

Superscript:

'	denotes conditions relative to a blade row

APPENDIX B

OPERATIONAL AND MECHANICAL EXPERIENCE

Because of the unique properties of liquid hydrogen, operational and mechanical problems were encountered during testing operations. The source of these problems was traced back to design, construction, and operational techniques. It is felt that a discussion of the operational and mechanical experience obtained in this investigation will be of interest to the reader.

In the design of the pump package (fig. 10) neoprene O-rings were used to seal flanges at atmospheric temperature. Stainless-steel O-rings were used in flanges at or near liquid-hydrogen temperature. Some of the stainless-steel O-rings did not seal satisfactorily because of surface imperfection. In order to assure perfect seals at every assembly, the metal O-rings were replaced and plated with silver (0.0006 to 0.0008 in.), which formed an adequate seal surface when the O-ring was compressed.

Carbon face seals running against the pump inlet shroud surface, back surface of the pump, and on the pump side of the lower bearing were found to wear excessively. A carbon with an impregnated lubricant was substituted and found to extend seal life considerably when the contact surface was 304 stainless steel. Face-seal failures also occurred because of bearing-oil lubricant on the seal surfaces, which were near liquid-hydrogen temperatures. These failures were stopped at the expense of decreased bearing life by lubricating both bearings with a low-temperature grease. Performance of the two face seals above the pump rotor was also improved when the gas pressure between the seals was regulated.

Resistance-type heating coils around the outer diameter of the bearing housing were used to increase temperature to that required by the bearing lubricant. This additional heat was not enough, however, to prevent the lower bearing outer race from shrinking and brinelling the contact surface. Bearing performance improved considerably when radial clearances were increased to 0.0006 to 0.0010 inch (standard radial clearance is 0.0002 to 0.0006 in. for this size bearing).

Vacuum-jacketed piping utilized in this investigation employed a single "warm" gas seal bayonet-type joint. Because of excessive clearances between mating bayonet joints, leaks developed that did not occur when the system was pressure-checked at ambient temperature and liquid-nitrogen temperature. Teflon spacers and rugged bolt-type flange clamps stopped further seal failures at pipe flange joints.

Before hydrogen (liquid or gas) was introduced into the test system, the system was thoroughly purged. The purge method consisted of evacuating the system to 25 inches of mercury and pressurizing with helium gas to 10 pounds per square inch gage. Complete purging was assured by repeating this process. A constant flow of nitrogen gas (2 psig) through the main vent line leading to the burner head was started during the second system purge and maintained during testing operation in order to keep air from entering the vent system. When the system was under helium pressure, the tubing connecting pressure taps and transducers was also purged by bleeding the lines at the tubing connectors near the pressure transducers.

During the pump operation, temperature stratification in the liquid-hydrogen Dewar was observed. This was due to the temperature rise from pump energy addition and heat leak into the flow system, which resulted in a decrease in density of the fluid returning to the top of the Dewar. The low-density hydrogen apparently remained stratified in the Dewar under the operating conditions of flow and pressure. This phenomenon was manifested in two ways. First, in order to maintain a moderate tank pressure (20 psig) during pump operation, it was necessary to bleed sizable quantities of hydrogen vapor from the Dewar. Secondly, the pump inlet temperature remained at about 37° R until almost the entire volume had been pumped through the cycle, after which the inlet temperature rose very quickly to the vapor-pressure conditions in the tank. This step change in inlet conditions resulted in a large reduction in net positive suction head, and the pump became vapor-bound. Thus, such test loops cannot be designed assuming the fluid to be at uniform equilibrium conditions in the Dewar.

REFERENCES

1. Ross, C. C., and Banerian, Gordon: Some Aspects of High-Suction Specific-Speed Pump Inducers. Trans. ASME, vol. 78, no. 8, Nov. 1956, pp. 1715-1721.

2. Stanitz, John D., and Ellis, Gaylord O.: Two-Dimensional Compressible Flow in Centrifugal Compressors with Straight Blades. NACA Rep. 954, 1950. (Supersedes NACA TN 1932.)

3. Smith, Kenneth J., and Hamrick, Joseph T.: A Rapid Approximate Method for the Design of Hub-Shroud Profiles of Centrifugal Impellers of Given Blade Shape. NACA TN 3399, 1955.

4. Hamrick, Joseph T., Ginsburg, Ambrose, and Osborn, Walter M.: Method of Analysis for Compressible Flow Through Mixed-Flow Centrifugal Impellers of Arbitrary Design. NACA Rep. 1082, 1952. (Supersedes NACA TN 2165.)

5. Hamrick, Joseph T., Beede, William L., and Withee, Joseph R., Jr.: Design and Test of Mixed-Flow Impellers. IV - Experimental Results for Impeller Models MFI-1 and MFI-2 with Changes in Blade Height. NACA RM E53L02, 1954.

6. Shepherd, D. G.: Principles of Turbomachinery. The Macmillan Co., 1956.

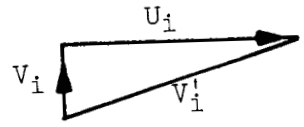

(a) Inlet velocity diagram.

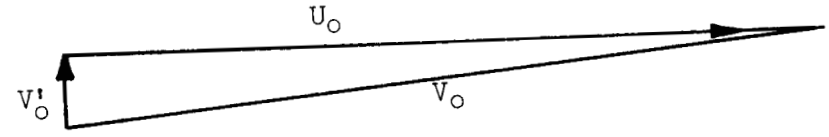

(b) Outlet velocity diagram.

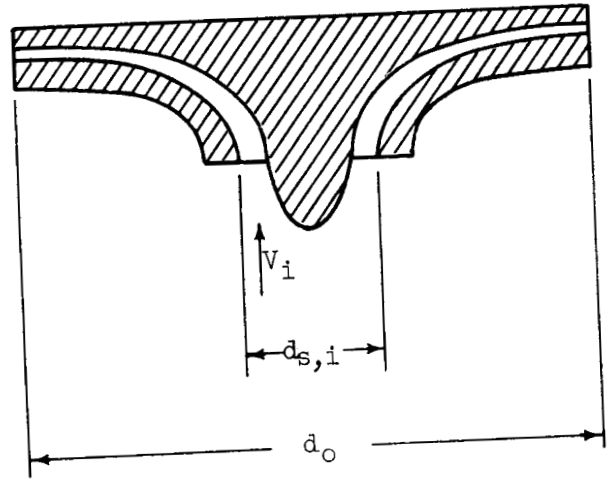

(c) Pump geometry.

Figure 1. - Tip velocity diagrams and geometry for radial outlet pump.

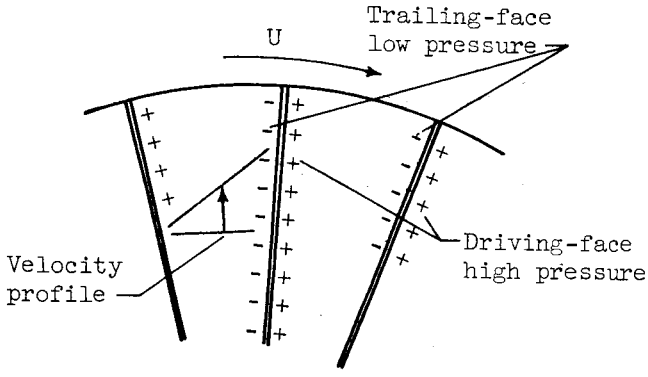

(a) Desired through-flow velocity and pressure conditions.

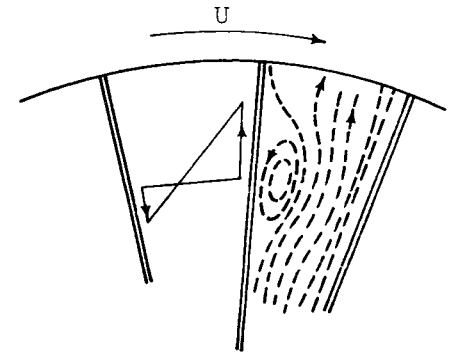

(b) Eddy or reverse flow.

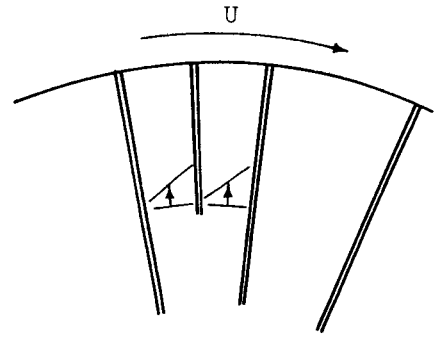

(c) Splitter vanes to avoid eddy condition.

Figure 2. - Pressure and velocity distributions in radial pump.

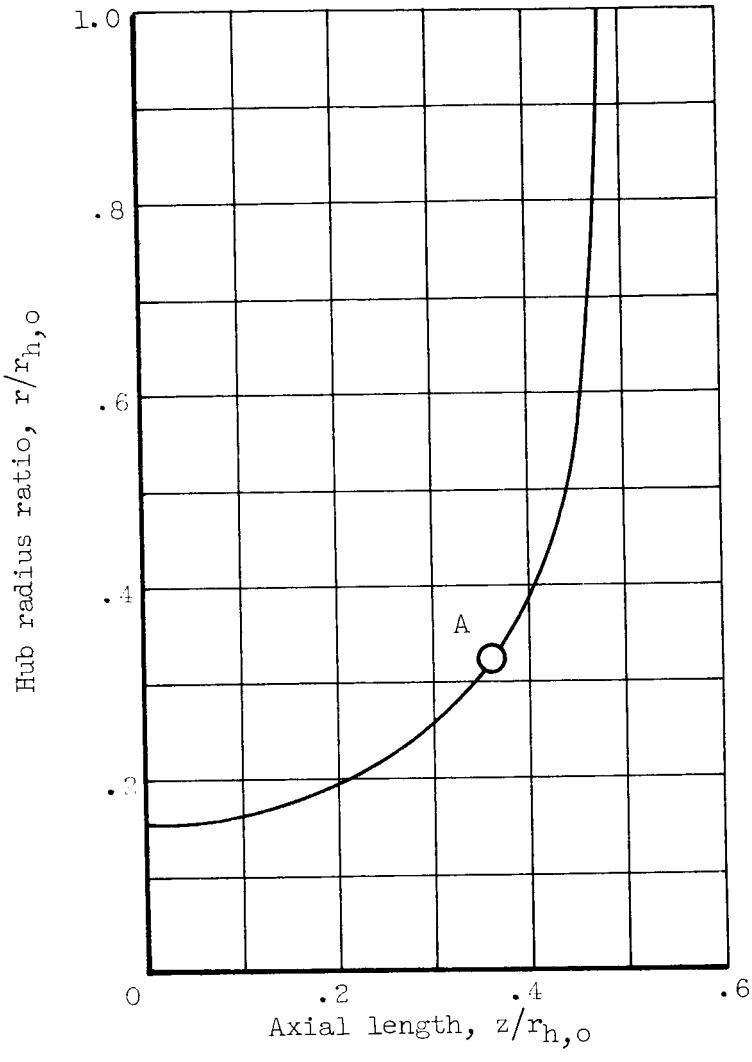

(a) Hub contour.

Figure 3. - Centrifugal-pump hub specifications.

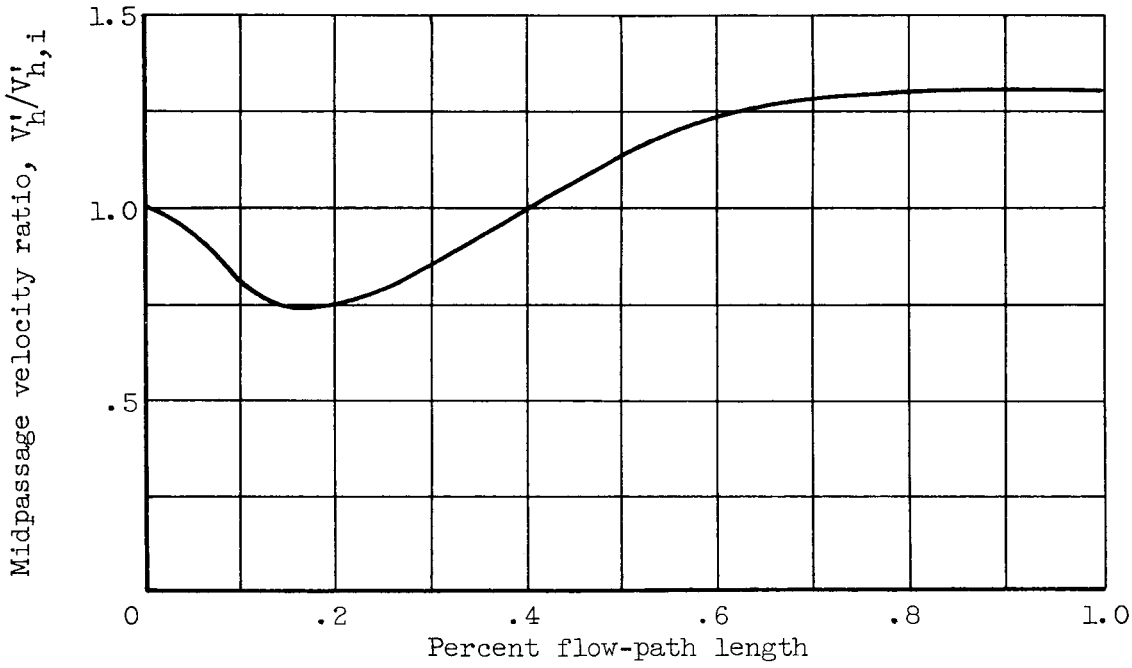

(b) Hub relative-velocity distribution.

Figure 3. - Concluded. Centrifugal-pump hub specifications.

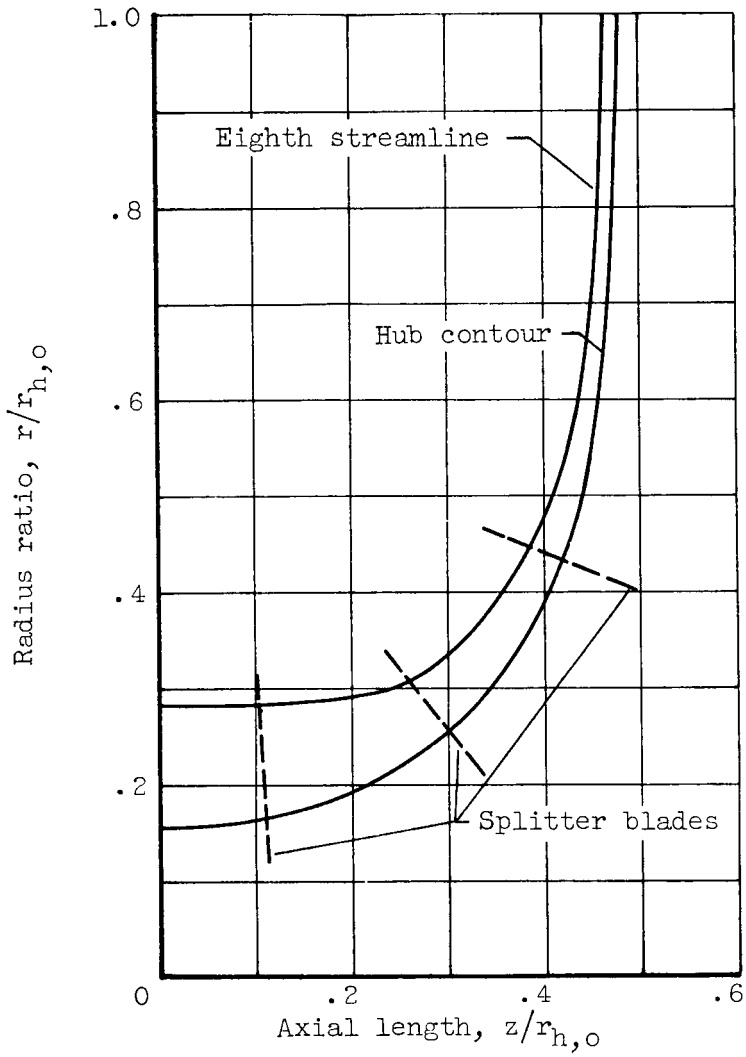

Figure 4. - Hub and calculated shroud contours.

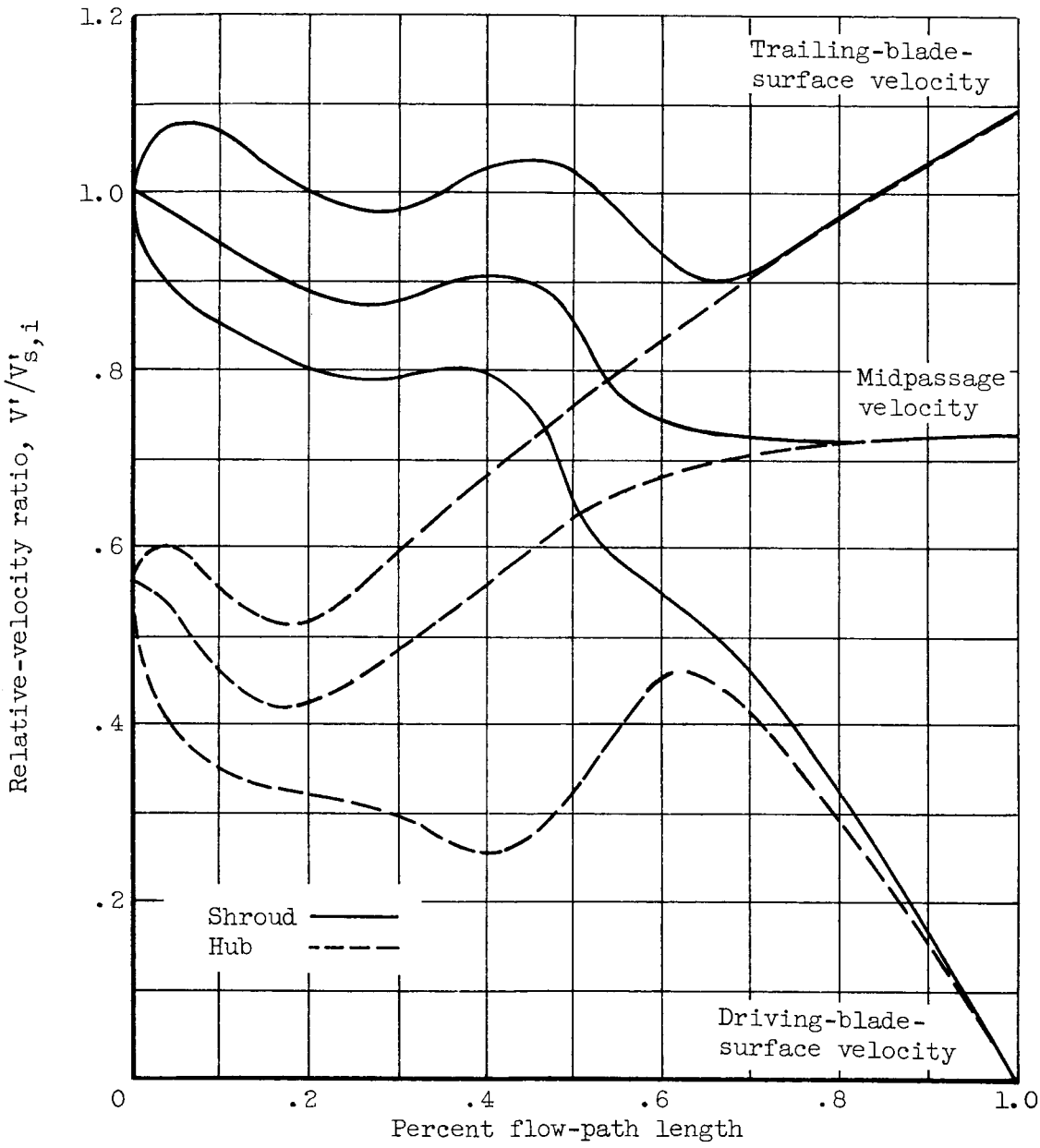

Figure 5. - Design hub and shroud relative velocities of a centrifugal pump rotor.

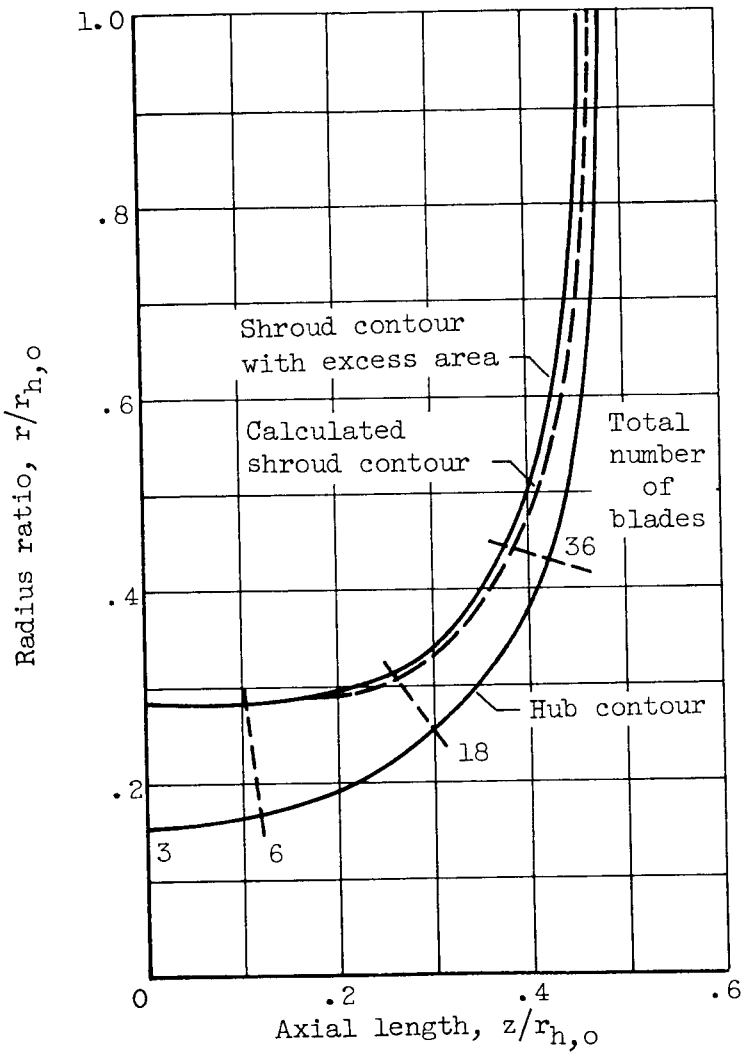

Figure 6. - Design hub-shroud contours and area allowance contour for a centrifugal pump rotor.

z, in.	r_h, in.	r_s, in.	θ
0	0.312	0.570	0°
.06	.314		21°05'
.12	.319		40°21'
.18	.328		57°46'
.24	.338		73°22'
.30	.354	.570	87°07'
.36	.373	.575	99°03'
.40		.590	105°59'
.42	.398	.599	109°09'
.48	.428	.625	117°24'
.54	.468	.663	123°51'
.60	.514	.715	128°27'
.66	.572	.781	131°13'
.72	.649	.875	132°0'
.90	1.090	1.570	132°0'
.96	2.000		132°0'

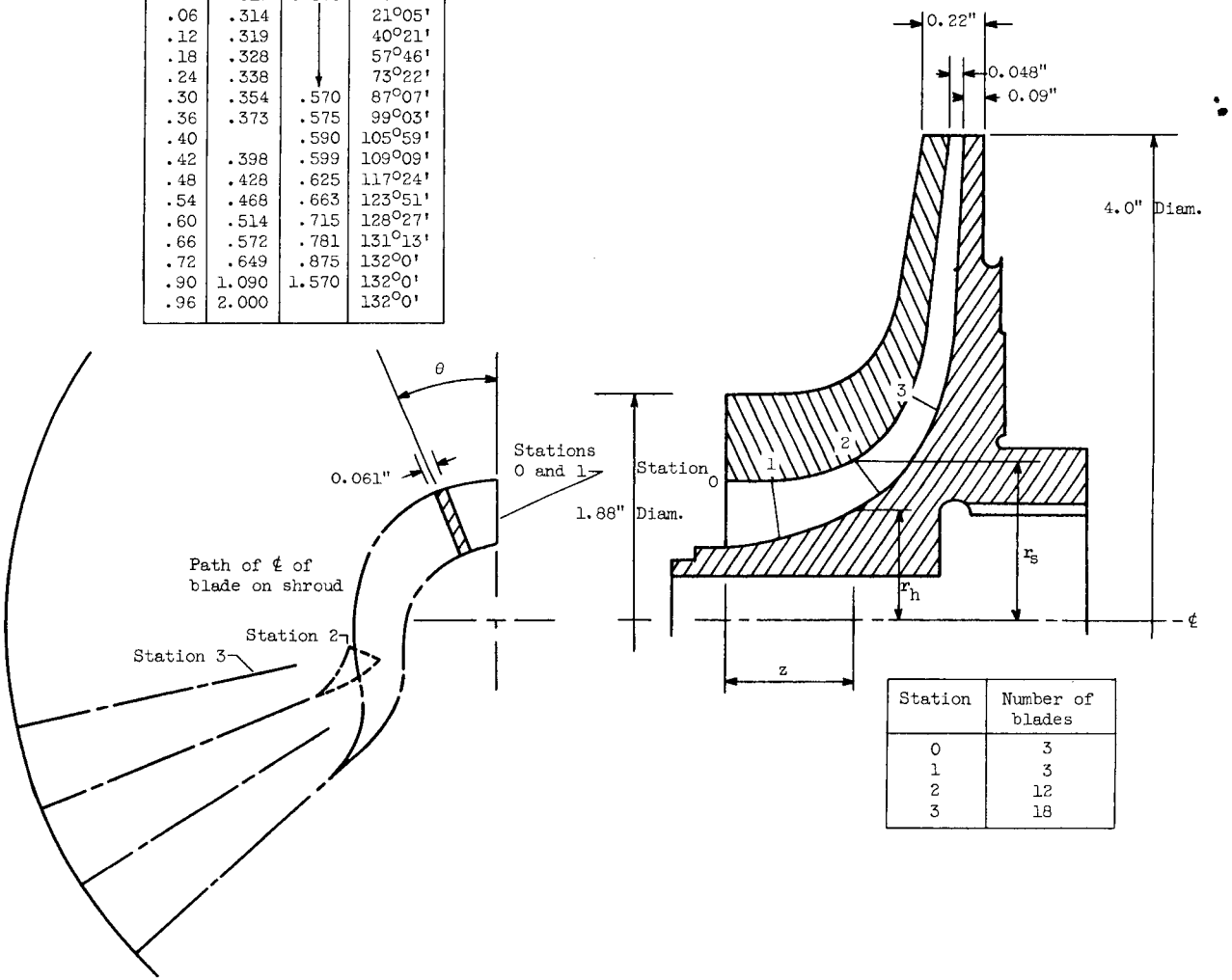

Station	Number of blades
0	3
1	3
2	12
3	18

Figure 7. - Sketch of 4-inch-diameter centrifugal pump rotor and blade coordinates.

Figure 8. - Photograph of shrouded and unshrouded pump impellers.

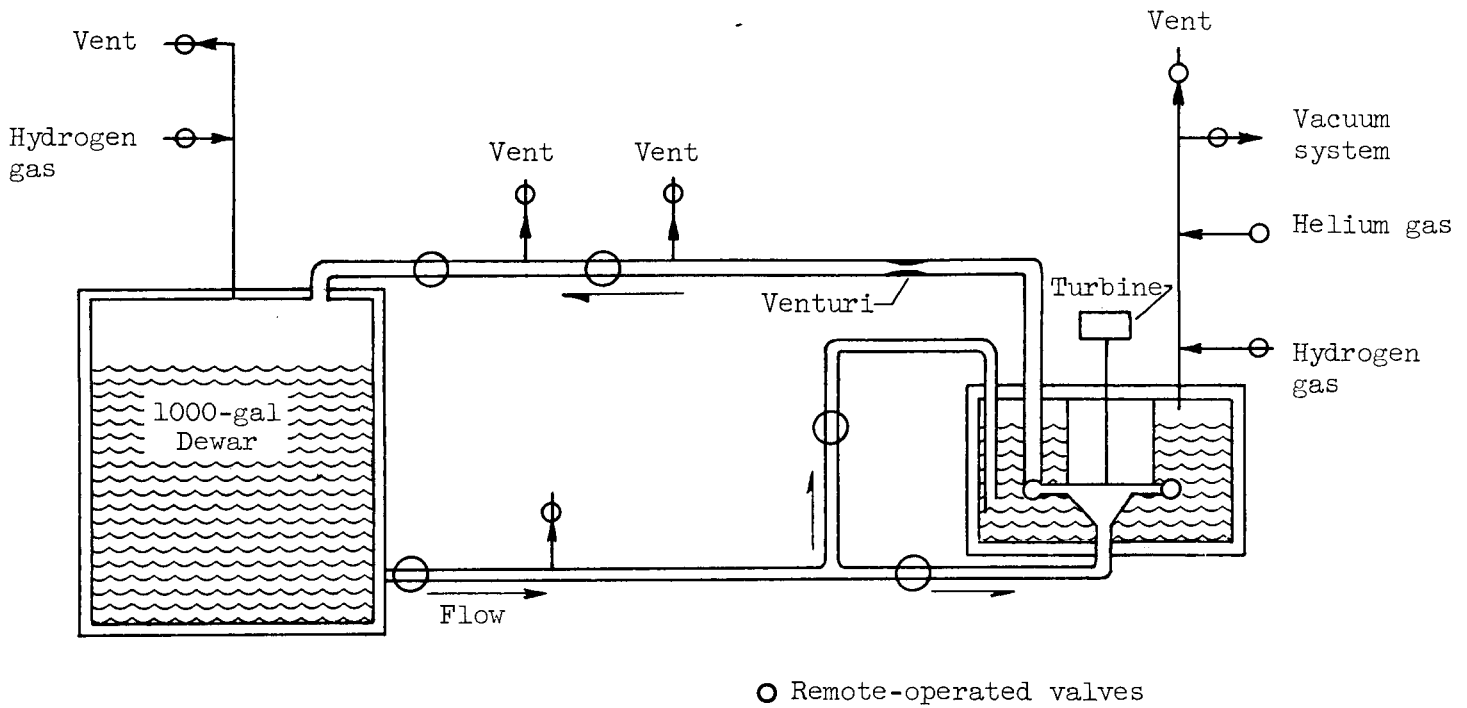

Figure 9. - Schematic of liquid-hydrogen-pump test facility.

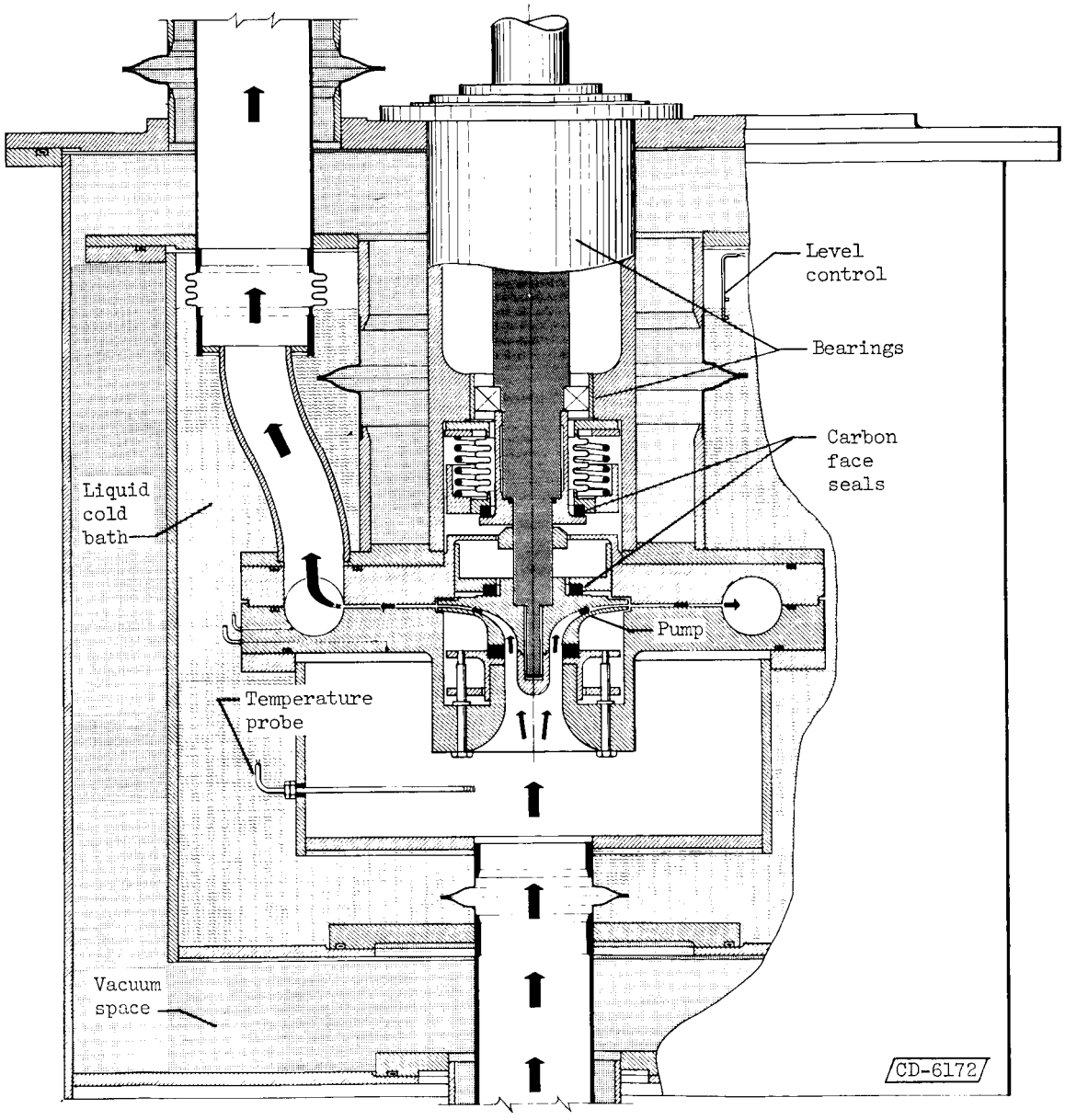

Figure 10. - Schematic of pump assembly.

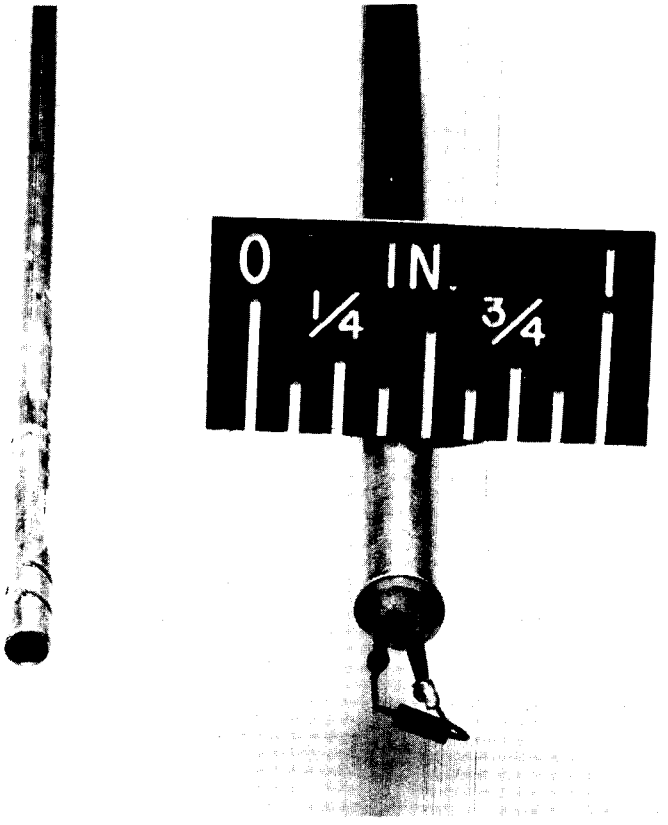

C-48473

(a) Shielded temperature probe.

(b) Level indicator.

Figure 11. - Typical carbon resistor probes.

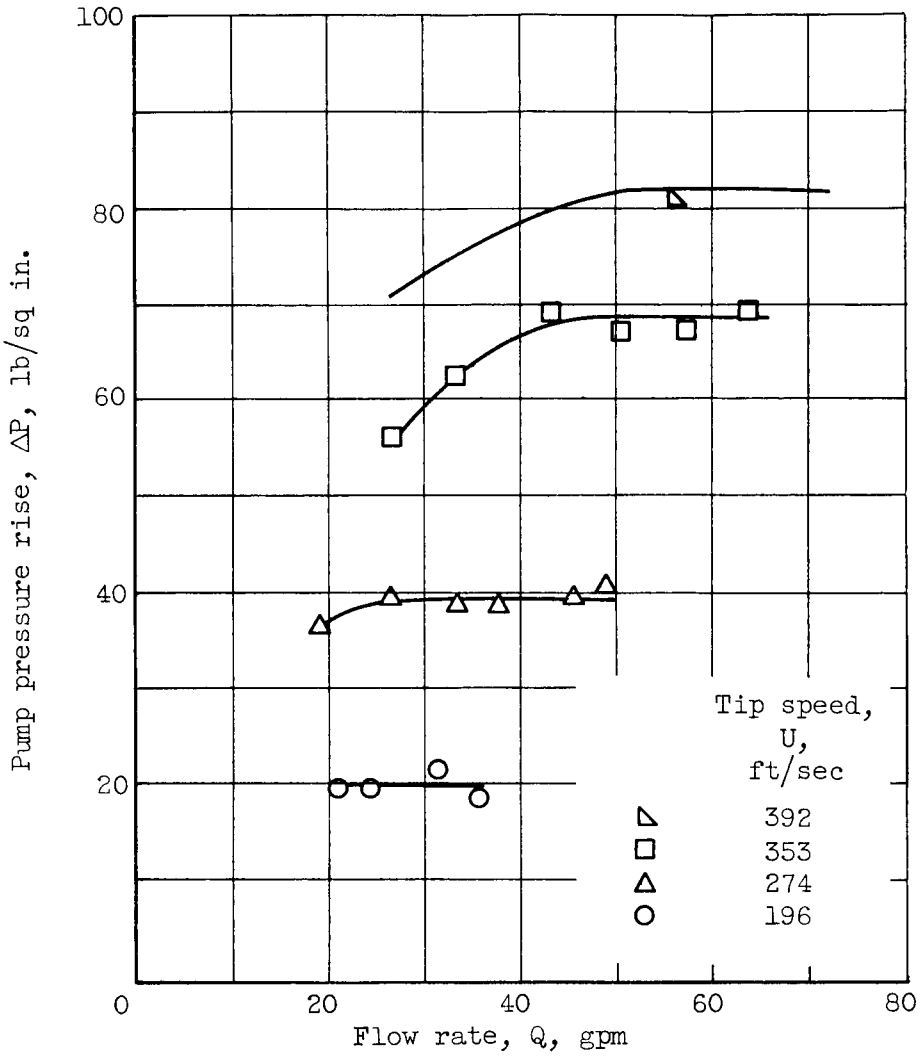

Figure 12. - Shrouded centrifugal-pump performance in liquid hydrogen.

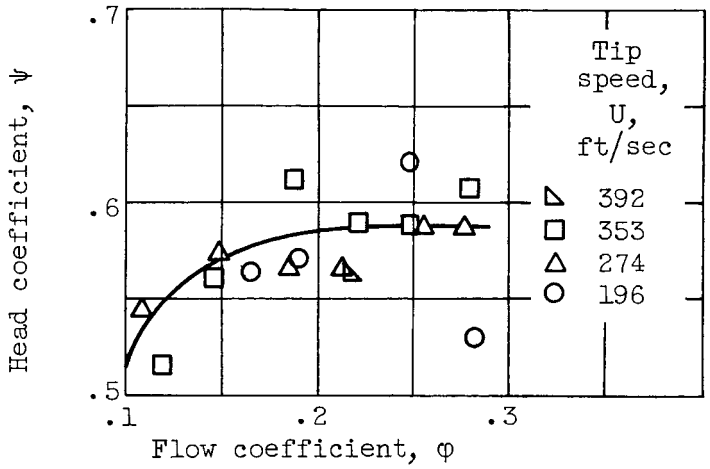

Figure 13. - Pump similarity performance.

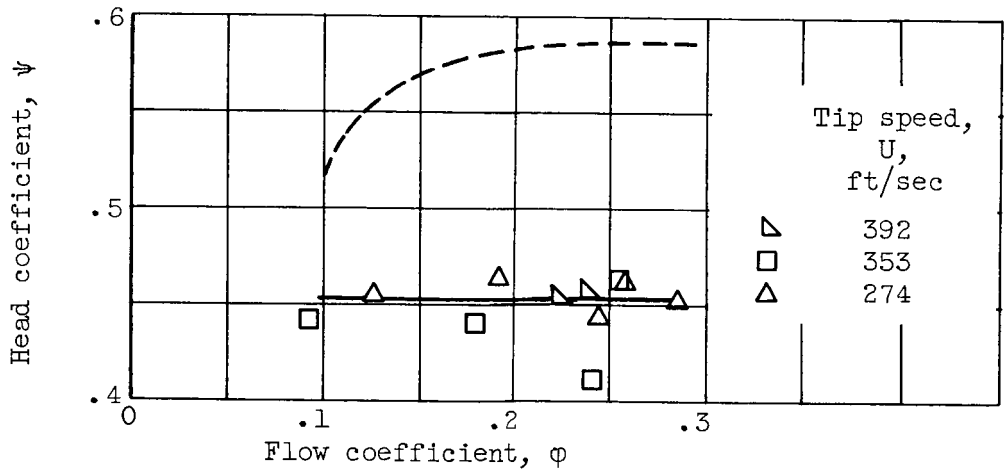

Figure 14. - Performance comparison of shrouded and unshrouded pumps in liquid hydrogen.